

# Production of Sub-MeV Positive Gold Ion Beams with Various Gas Targets to Improve the Tandem Accelerator of the LHD-HIBP

Akira TANIIKE, Takeshi IDO<sup>1)</sup>, Masaki NISHIURA<sup>1)</sup>, Akihiro SHIMIZU<sup>1)</sup>,  
Yuichi FURUYAMA and Akira KITAMURA

*Graduate School of Maritime Sciences, Kobe University, Kobe 658-0022, Japan*

<sup>1)</sup>*National Institute for Fusion Science, Toki 509-5292, Japan*

(Received 8 December 2009 / Accepted 30 March 2010)

To expand the application range of heavy ion beam probe measurement in the Large Helical Device (LHD), it is important to increase the probing beam current. The current can be increased by improving the charge exchange efficiency in a gas cell. Experiments were conducted on a tandem accelerator at Kobe University, 5SDH-2, which allows various experimental conditions such as gas species, gas pressure, and beam energy to be selected. Initially, the gas thickness was determined by a beam attenuation method with a He<sup>+</sup> ion beam. Next, the dependence of the positive beam current on the gas thickness was measured. The ionic charge fraction of the accelerated beam was measured and compared with the value calculated using the ionization cross section calculated in [M. Nishiura *et al.*, NIFS Report, NIFS-884 (2008)]. The dependence of the Au<sup>+</sup> fraction on the target gas thickness shows good qualitative agreement with the experimental value. However, the cross sections obtained experimentally are several times larger than those calculated.

© 2010 The Japan Society of Plasma Science and Nuclear Fusion Research

Keywords: Au<sup>-</sup> ion beam, gas cell, ionization, tandem accelerator, HIBP, LHD

DOI: 10.1585/pfr.5.S2087

## 1. Introduction

It is important to increase the probing beam current in order to expand the application range of heavy ion beam probe measurement in the Large Helical Device (LHD-HIBP) [1]. Some methods for increasing the current are considered. One method is to improve the charge exchange efficiency at a gas cell in the tandem accelerator of the LHD-HIBP. Another is to increase the negative beam current [2]. It is difficult to conduct a charge exchange experiment with various gas species and gas pressures in a gas cell in the LHD-HIBP accelerator.

The objective of this study is to examine the physics of atomic collisions between Au<sup>-</sup> ions and atoms introduced into a gas cell at a high-voltage terminal. Energy of 150 kV was chosen for the Au<sup>-</sup> ions. Because the energy is lesser than that of the LHD-HIBP, a theoretical model with collision cross sections for a wide range of ion energies is needed. Experimental results corresponding to the collision cross sections are obtained in this work by applying the experimental results to the model. Using the model, the target gas can be optimized to increase the Au<sup>+</sup> beam current, extending the applicable range of the LHD-HIBP.

## 2. Experiment

### 2.1 Experimental apparatus

The experiments were conducted on a tandem Van de Graaff accelerator at Kobe University, 5SDH-2. The ac-

celerator has five beam lines, the M45, M30, M15, P15, and P45 lines, and has been used for accelerator analyses such as Rutherford backscattering spectroscopy, elastic recoil detection analysis, nuclear resonance analysis, and particle-induced X-ray emission, as well as ion beam irradiation for material modification. This accelerator uses a gas cell for charge stripping of the accelerated ions and is of the same type as the LHD-HIBP's accelerator. The maximum terminal voltage of 5SDH-2 is 1.7 MV, and that of the LHD-HIBP is 3.0 MV. Using the 5SDH-2 accelerator, experiments can be conducted with various gas species, gas pressures, and beam energies. The accelerator can generate Au<sup>+</sup> ion beams as well as many other ion beams, and a reference experiment can be conducted using the beams. Unfortunately, the momentum of MeV Au ions is too large to be bent by a bending magnet, or the SW magnet, of the 5SDH-2 system, even on the M15 beam line, which has the smallest deflection angle. Therefore, the terminal voltage is limited to about 150 kV.

Figure 1 shows a schematic view of the accelerator, two ion sources, and the beam line components. A Faraday cup (FC) with a pair of Sm-Co magnets is installed in an end chamber of the M15 beam line to measure the beam current. Although the FC's collector can be biased to a potential of +240 V with a dry battery, the beam current was observed to be unchanged with the application of the bias. This indicates that the magnets work effectively to suppress emission of secondary electrons generated by ion

author's e-mail: taniike@maritime.kobe-u.ac.jp

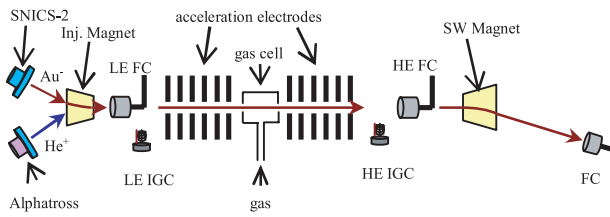


Fig. 1 Schematic view of experimental apparatus.

incidence. Most experiments in this work were conducted with biasing, and occasionally without biasing.

The accelerator has an  $N_2$  gas cylinder outside the accelerator tank; gas is introduced through a tube into a gas cell. In this work, the tube was branched with a T connector. By connecting a gas cylinder to the T connector, various gases can be introduced.  $H_2$ , He, Ne, Ar, and Xe gas were used in this work. A gas cell for charge stripping is placed between the acceleration tubes; the entrance and exit apertures are 7.9 mm in diameter, and the length of the separation is 610 mm. A turbo molecular pump is installed in the cell system to raise the confinement of the introduced gas. The gas pressure was measured by two ion gauge controller (IGC) at the low-energy (LE) and high-energy (HE) side beam lines of the tandem accelerator. The base pressures were subtracted from the two gas pressure values, and the two resulting values were averaged. Because the gas pressure at the LE IGC was affected by the working gas at the ion source and/or by outgassing from the ion source, the value of the HE IGC was adopted as the gas pressure. The value of the base pressure was subtracted, and the result was corrected by the sensitivity coefficients of the gas gauge. As the value was proportional to the effective gas pressure in a gas cell, the value was calibrated to the gas pressure in a gas cell by the beam attenuation method described in section 2.2.

A  $Au^-$  ion beam was generated by the SNICS-2 ion source. The beam current was typically 100 nA at the LE FC. The extraction voltage was  $-21$  kV. The voltage was small in the case of  $H^-$  extraction, typically  $-28$  kV. This was because the power supply load of the bending magnet was decreased to select the ion source.

Alphasross ion source is of the RF discharge type, and it generates a  $He^+$  ion beam. This ion source is usually used for  $He^-$  ion beam generation by charge exchange with a Rb vapor cell. In this work, the Rb charge exchange cell was not used. Two power supplies for extraction and lensing were replaced from a negative bias to a positive one, and a  $He^+$  ion beam with an energy of 21 keV was extracted. This beam was used in the beam attenuation method described in section 2.2.

## 2.2 Determination of gas thickness

Determination of the absolute gas thickness is crucial to discussing cross sections and charge fractions. The value was determined by a beam attenuation method in this

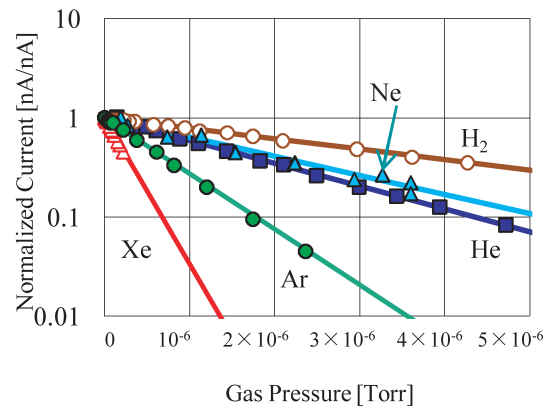


Fig. 2 Experimental and calculated beam attenuation curves.

work. The  $He^+$  ion beam described above was used for this method. The ion beam was transported to the FC at the end chamber through two acceleration tubes on the LE and HE sides and a gas cell. Gas was introduced into the gas cell, and an attenuated ion beam was investigated. Moreover, various gases were used.

The number of He ions decreases with the introduction of gas into the gas cell. The decrease curve is represented by certain cross sections. An ionization cross section,  $\sigma_{1,2}$ , a recombination cross section,  $\sigma_{1,0}$ , and a scattering cross section are considered. The values of  $\sigma_{1,0}$  and  $\sigma_{1,2}$  for He, Ne, and Ar gas targets were given in Ref. [3], and that for a Xe gas target was assumed from these values. Because each  $\sigma_{1,2}$  value is negligibly smaller than  $\sigma_{1,0}$ ,  $\sigma_{1,2}$  is not used in these calculations. The scattering cross section  $\sigma_s$  was calculated using a Biersack–Ziegler universal potential, and the procedure was described in Ref. [4]. The limit of the scattering angle is determined by the geometry of the gas cell and the FC at the end chamber. For a  $H_2$  target, all projectiles are detectable, and  $\sigma_s$  is zero. Otherwise, the  $\sigma_s$  value obtained from the above calculation was negligibly smaller than  $\sigma_{1,0}$ . To obtain the exact beam attenuation curve, the charge fraction must be calculated. Some rate equations were calculated, and the contribution of neutral He and  $He^{2+}$  ions was found to be small for thin targets. As a result, the attenuation curve was fit simply by the following equation.

$$I = I_0 \exp\{-(\sigma_{1,0} + \sigma_{1,2} + \sigma_s) nl\}, \quad (1)$$

where  $nl$  is gas thickness.

Figure 2 shows the experimental results of the beam attenuation method. The beam current was normalized by the value at the lowest pressure. The calculated results from Eq. 1 are also shown. A gas pressure calibration factor  $f$  was obtained by fitting the calculated values to the experimental data for the He target curve. The factors were 502, 516, 325, 868, and 1870 for  $H_2$ , He, Ne, Ar, and Xe targets, respectively. The errors in fitting were typically several tens of percent and were 35% for the Ne target. These factors show the ratio of the gas pressure outside the accelerator and that in the gas cell. The conductance of

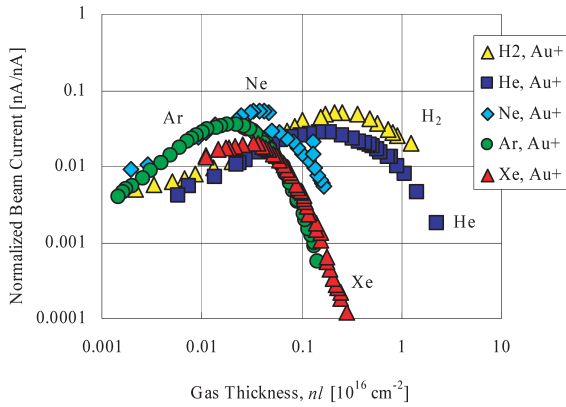


Fig. 3  $\text{Au}^+$  beam current dependence on gas thickness. Various gases are used as targets.

the vacuum component is proportional to the average atom velocity. Because the average velocity for a heavy gas is smaller than that for a light gas, the factor is large. The tendency agrees with the fitting results.

Thus, the gas thickness  $nl$  is given by

$$nl = 3.30 \times 10^{16} \times P \times f \times 61.0 [\text{cm}^{-2}], \quad (2)$$

where  $P$  is the gas pressure measured by a ionization gas gauge in Torr. The factor of  $3.30 \times 10^{16} \text{ cm}^{-3}$  is the density of atoms or molecules at  $20^\circ\text{C}$  and 1 Torr.

### 2.3 Fraction measurements

$\text{Au}^-$  ion beams were injected into the accelerator, and output beams such as  $\text{Au}^+$ ,  $\text{Au}^{2+}$ , and  $\text{Au}^{3+}$  ion beams were measured by the LE- and HE-side FCs at the end chamber of the accelerator. The  $\text{Au}^{2+}$  and  $\text{Au}^{3+}$  ion beam currents were too small for ion detection; in some cases, these currents could not be detected. In other cases, these currents could be measured; although they were one or two orders of magnitude smaller than that of the  $\text{Au}^+$  ion beam, these values could provide information on the gas thickness dependence of the current.

The beam current at the LE FC was almost stable in one run but varied during another. The beam current measured by the FC at the end chamber was normalized by the LE FC current and the ion's charge state. The comparison of measured currents at the FC was used to normalize the currents in particle-nA/nA.

The energy of  $\text{Au}^-$  ions incident on the gas cell was 150 keV. The energy of ions from a negative source was 21 keV, and the tandem acceleration voltage was 129 kV. The energies of positive ions were 279 keV for  $\text{Au}^+$ , 408 keV for  $\text{Au}^{2+}$ , and 537 keV for  $\text{Au}^{3+}$ .

Figure 3 shows the dependence of the Au beam current on the gas thickness in the gas cell.  $\text{H}_2$ , He, Ne, Ar, and Xe gases were used as target gases. The peak values of the normalized current are almost the same; the differences are within a factor of two. The gas thickness at the peak of the normalized current is large for small target atoms.

Figure 4 shows the dependence of  $\text{Au}^+$ ,  $\text{Au}^{2+}$ , and

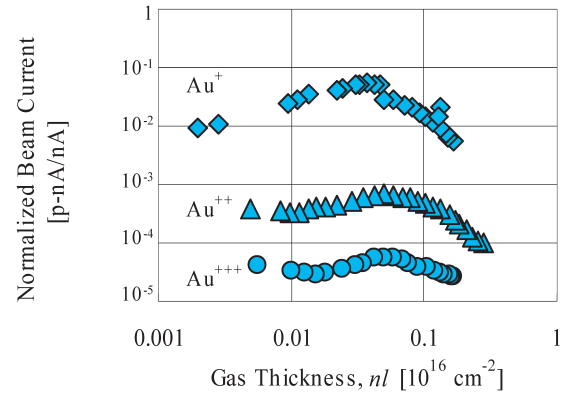


Fig. 4  $\text{Au}^+$ ,  $\text{Au}^{2+}$ , and  $\text{Au}^{3+}$  beam current dependence on gas thickness for a Ne target.

$\text{Au}^{3+}$  beam currents on gas thickness for a Ne gas target. The current of the  $\text{Au}^{2+}$  and  $\text{Au}^{3+}$  ion beams were too small, of the order of pA, but the dependence of the current on the gas thickness was obtained. The gas thicknesses at the peak of the charge states were almost the same.

### 3. Comparison of Measured and Calculated Charge Fraction

The charge fraction can be calculated by solving the rate equations as described in Ref. [5]. The cross sections described in Ref. [4] are used; they are listed in Table 1. To estimate the fractions of  $\text{Au}^-$ ,  $\text{Au}^0$ ,  $\text{Au}^+$ , and  $\text{Au}^{2+}$ ,  $\text{Au}^-$ ,  $\text{Au}^0$ ,  $\text{Au}^+$ ,  $\text{Au}^{2+}$ ,  $\text{Au}^{3+}$ ,  $\text{Au}^{4+}$ , and  $\text{Au}^{5+}$  are considered in the calculation. Note that the estimated fractions of  $\text{Au}^{3+}$ ,  $\text{Au}^{4+}$ , and  $\text{Au}^{5+}$  were incorrect, because some cross sections for higher charge states were not used. The results are shown in Fig. 5.

The shape of the calculated curve in Fig. 5 is in good agreement with that of the experimental curve shown in Fig. 3. However, the calculated Au fraction has a peak at a gas thickness of  $10^{15} \text{ cm}^{-2}$ , but the measured fraction has a peak at a gas thickness of  $2.6 \times 10^{14} \text{ cm}^{-2}$ . That is, the measured cross section is four times the calculated one. This discrepancy may be caused by uncertainty in the gas thickness measurement. For example, considering the dependence of the conductance on the thermal velocity of gas atoms/molecules, the factor  $f$  for the Ar target is estimated to be at 1500. Thus, the measured cross sections are three times the cross section estimated in Ref. [4] and are six times the cross section shown in Ref. [6]. We should verify the validity of the pressure measurement, including the dependence of the sensitivity on gas species. The pressure gradient in the columns should also be considered. Installing a gas gauge at the gas cell is a definitive way to determine the local gas pressure. However, it is difficult because the gas cell is located on a high-voltage terminal. Instead,  $\text{H}_2$  target experiments will provide us reliable data on the gas thickness because of the small scattering cross section and well-known ionization cross sections.

Table 1 Cross sections used to calculate the charge fraction (units  $10^{-16} \text{ cm}^2$ ).

$\sigma_{-1,0}$	16.77	/	/	/	/	/	/
$\sigma_{-1,1}$	6.90	$\sigma_{0,1}$	7.83	/	/	/	/
$\sigma_{-1,2}$	2.84	$\sigma_{0,2}$	3.00	$\sigma_{1,2}$	4.85	/	/
$\sigma_{-1,3}$	2.08	$\sigma_{0,3}$	2.14	$\sigma_{1,3}$	2.42	$\sigma_{2,3}$	2.57
/	/	$\sigma_{0,4}$	1.21	$\sigma_{1,4}$	1.37	$\sigma_{2,4}$	1.70
/	/	/	/	/	/	$\sigma_{2,5}$	1.05

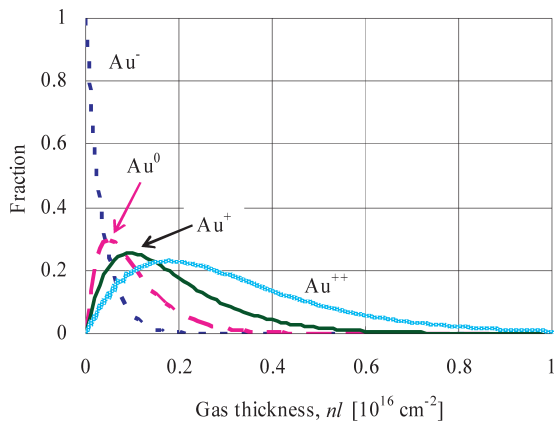


Fig. 5 Fraction calculations for Au ions colliding with Ar target. Incident energy of  $\text{Au}^-$  ions is 150 keV.

### 4. Summary

The gas thickness in the 5SDH-2 system was determined by a beam attenuation method with a  $\text{He}^+$  ion beam. Then, experiments with different gas species and gas pressures were conducted. The dependence of the beam current on gas thickness was measured for a 150-keV  $\text{Au}^-$  ion beam. The charge fraction was calculated by solving rate equations. The dependence of the  $\text{Au}^+$  fraction on the target gas thickness is in good qualitative agreement with the experimental result. However, the cross sections obtained experimentally are several times larger than those described in Ref. [4, 6]. This discrepancy may be caused by uncertainty in the gas thickness measurement.

### Acknowledgements

We thank Dr. H. Tawara and Professor V. P. Shevelko for their advice regarding our experiments. This work was supported by NIFS grant NIFS08KCHB002 (2008-2009).

- [1] T. Ido *et al.*, Rev. Sci. Instrum. **77**, 10F523 (2006).
- [2] M. Nishiura *et al.*, Rev. Sci. Instrum. **79**, 02C713 (2008).
- [3] M. E. Rudd *et al.*, Phys. Rev. A **32**, 2 (1985).
- [4] M. Nishiura *et al.*, NIFS Report, NIFS-884 (2008).
- [5] A. Taniike *et al.*, Fusion Eng. Des. **34-45**, 675 (1997).
- [6] M. M. Sant' Anna *et al.*, Plasma Phys. Control. Fusion **51**, 045007 (2009).